Eur. Phys. J. B **74**, 177–193 (2010)
DOI: 10.1140/epjb/e2010-00073-x

THE EUROPEAN PHYSICAL JOURNAL B

Regular Article

Noise-induced synchronization in bidirectionally coupled type-I neurons

N. Malik[1], B. Ashok[2], and J. Balakrishnan[3,a]

[1] Potsdam Institute for Climate Impact Research, Telegrafenberg, 14412 Potsdam, Germany
[2] Advanced Centre for Research in High Energy Materials (ACRHEM), University of Hyderabad, Central University PO, Gachi Bowli, Hyderabad - 500 046, India
[3] School of Physics, University of Hyderabad, Central University PO, Gachi Bowli, Hyderabad - 500 046, India

Received 4 June 2009 / Received in final form 22 November 2009
Published online 9 March 2010 – © EDP Sciences, Società Italiana di Fisica, Springer-Verlag 2010

Abstract. We present here some studies on noise-induced order and synchronous firing in a system of bidirectionally coupled generic type-I neurons. We find that transitions from unsynchronized to completely synchronized states occur beyond a critical value of noise strength that has a clear functional dependence on neuronal coupling strength and input values. For an inhibitory-excitatory (IE) synaptic coupling, the approach to a partially synchronized state is shown to vary qualitatively depending on whether the input is less or more than a critical value. We find that introduction of noise can cause a delay in the bifurcation of the firing pattern of the excitatory neuron for IE coupling.

1 Introduction

Among the host of interesting dynamical behaviour observed in coupled nonlinear systems, synchronization phenomena are one of the most fascinating and among the most studied. These phenomena abound in nature and in daily life: studies have been made of synchronization in numerous systems – in pendulum clocks, electronic circuits, chemical systems, swarms of light-emitting fireflies, biological rhythms, coupled Josephson junctions, cardiorespiratory interactions, neuronal ensembles in sensory systems, etc. to name a few. Synchronous activity in neuronal ensembles in particular, have received a great deal of attention and numerous studies have been done on the spiking patterns of neurons and neuronal networks [1–17]. Neuronal ensembles perform complex tasks and can extract different kinds of features from the information they receive and it is believed that cognitive tasks such as feature extraction and recognition, sensory perception, etc., are brought about by synchronous neuronal activity. The mechanisms and dynamics of synchronization phenomena in neurons are therefore of great interest [7–17].

Neurons are of many kinds (see for instance [18]), but they may be broadly classified into two types based on their excitability mechanisms. This classification of neurons on the basis of the firing patterns of the axons was first done by Hodgkin and Huxley in their classic work [1].

Neurons of type-II begin firing at a relatively high frequency through a subcritical Hopf bifurcation.

Type-I neurons however can fire at arbitrarily low frequencies at low values of the applied input current, and the frequency increases with increasing values of the input. The equations which describe type-I dynamics can be reduced to the canonical normal form for a saddle-node bifurcation [7]. In appropriate parameter regimes the system operates in the close vicinity of a saddle-node bifurcation on an invariant circle and this ensures repetitive firing. It is interesting to study type-I neurons as almost all mammalian neurons fall under this class of excitability.

A variety of synchronous phenomena occur in nonlinear systems [19], but among these, complete synchronization (henceforth referred to as CS) is perhaps one of the most interesting [20] as it brings about synchronization in the phases, frequencies and amplitudes of the signals. Although CS is widely believed to happen between identical systems, and CS between non-identical systems is not usually expected, we have shown in a different work [15] that in an ensemble of two hundred non-identical bidirectionally coupled type-I neurons with random strengths coupled in an all-to-all way, near complete synchronization does indeed unexpectedly occur under the influence of weak Gaussian white noise.

In fact, a more extensive study of noise-induced synchronous activity in a system of just two bidirectionally coupled identical (excitatory-excitatory) type-I neurons reveals that the noise-induced CS state gives way beyond a critical coupling and noise strength, to a desynchronized regime and then to subsequent locking to a different partially synchronized state. We find that the value of the critical coupling constant is proportional to the

[a] e-mail: janaki05@gmail.com; jbsp@uohyd.ernet.in

square root of the noise strength [15]. We were unable to achieve CS (noise-induced or otherwise) in a system of only two bidirectionally coupled non-identical inhibitory-excitatory neurons, although we showed in [15] that in a larger ensemble, non-identical neurons can exhibit noise-induced CS.

In their studies of type-I neurons coupled through time-dependent synapses, Börgers and Kopell [11,12] discussed the effects of random connectivity on synchronization and the PING mechanism in networks of excitatory (E) and inhibitory (I) neurons.

In this work, we report some interesting observations we have made in some computer studies of coupled generic type-I neurons when subject to weak additive Gaussian white noise. The dynamics of the synapses coupling the neurons are governed by ordinary differential equations which depend upon the outputs of the presynaptic neurons [11,12] – we have considered both EE and IE bidirectional couplings.

We find that the coupled system shows type-I firing pattern for EE coupling which suggests the existence of a contraction region close to the stable manifold of the saddle – CS can thus be expected in EE coupled systems. This firing pattern is not seen for all the coupled neurons in IE systems – the existence of a contraction region is therefore in question in this case, giving a good reason not to expect CS for IE couplings.

As pointed out in [15], noise-assisted CS occurs in EE (identical) systems in certain parameter regimes beyond which CS is destroyed but replaced by a different partially synchronized state.

For such a system, we obtain here the functional dependence between the critical value of the noise strength and the strength of synaptic coupling and the externally applied input at the point when desynchronization gives way to CS.

For the system of two coupled IE neurons, noise-assisted CS could not be achieved, but we find that noise induces locking to a partially synchronized state at higher coupling strengths and external input values. For the IE system, there exists a transition point at a critical external-input value before which desynchronization increases with increasing noise strength, and beyond which desynchronization decreases with increasing noise strength. We also report here noise-induced delay in the bifurcation point associated with the firing pattern of the excitatory neuron in the IE system. We suggest that the fast-slow relaxation dynamics of the neuronal inputs in IE systems make CS of the outputs hard to achieve.

We organize our presentation in the following way. In Section 2 we review the mathematical description of the mechanism of firing in type-I neurons and the framework for studying them when they are coupled. In Sections 3–5 we describe our study of the coupled system in the presence of (weak) Gaussian white noise for EE and IE bidirectional couplings (Sects. 4 and 5, respectively), separately.

For each type of coupling we make different studies to get insights upon the mechanisms governing synchronization. These are discussed in separate subsections: for an intuitive understanding of the dynamics underlying the approach to synchrony or order, in Section 4.1 we draw an analogy with the mechanical system of two damped nonlinear spring-mass systems coupled together. In Section 4.2, we describe our study of CS using plots between instantaneous frequencies and instantaneous phases of the inputs to the neurons and explain why these can be used as indicators of CS in coupled systems. In Section 4.3 we show how firing frequency-input plots for the coupled system can give indications of whether or not the coupled system is likely to show CS. The largest and second largest Lyapunov exponents have been calculated for the deterministic coupled system. In Section 4.4, we present our study of noise-induced variation of firing frequency. In the IE case, we show in the corresponding Subsection, the very interesting finding of noise-induced *delay* in the bifurcation associated with firing for the excitatory neuron. In Section 4.5, we present our study of variation of the synchronization error for CS, with noise strength, input, and coupling strength. We obtain useful functional relations between these for EE as well as for IE couplings. Results of similar studies are presented for IE coupling in Section 5; in Section 5.4 we report our very interesting observation of noise-induced delay of bifurcation associated with the neuronal firing. In Section 6, we show for EE coupling how the synchronization time varies with noise strength and suggest the possibility of exploiting the results for feature extraction. We conclude by summarizing the results of our work in Section 7.

2 Coupled theta neurons

In a type-I neuron, the mechanism of excitability comes about as follows [7,10]. For low values of the control parameter (the input current), there is a stable fixed point and an unstable fixed point which is a saddle. Trajectories forming the unstable manifold leave the saddle point and enter the stable fixed point, forming a loop in phase space. This closed loop therefore now contains the stable and unstable fixed points. As the value of the control parameter is increased, the two fixed points come closer together, and at the critical value, they coalesce and then disappear, resulting in a stable periodic solution corresponding to repetitive firing.

The activity x_i of the ith type-I neuron in an ensemble of N neurons, can be related to the membrane conductance and its dynamics can be described by:

$$\dot{x}_i = x^2 + I_i, \qquad I_i = \beta_i + \sum_{j=1}^{N} \alpha_j g_{ji} s_{ji}, \tag{1}$$

where we have chosen to work in units in which the time constant for the membrane potential is set to unity [7,10]. Its total input I_i comprises of the external input β_i (which in this work we have taken to be constant), and the contributions from the presynaptic neurons, with $i = 1, \ldots, N$. The synaptic gating variable s_{ij} represents the fraction of ion channels open in the jth presynaptic neuron, and its

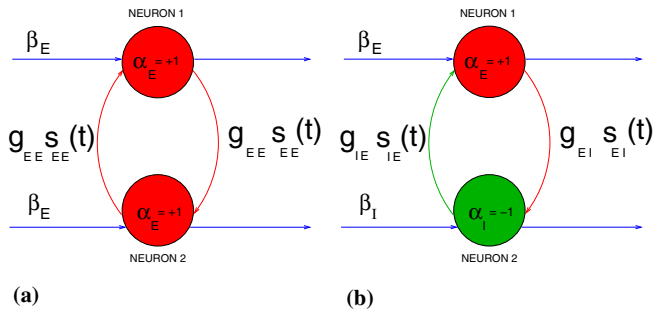

Fig. 1. (Color online) Bidirectional coupling between two theta neurons. Left: E-E coupling, right: I-E coupling.

values always lie in the range 0 to 1, reaching the maximal value when the neuron spikes. $\alpha_j = +1$ denotes an excitatory synapse and $\alpha_j = -1$ models an inhibitory synapse, while g_{ji} denotes the measure of the synaptic strength from neuron j to neuron i; in our work we have considered $g_{ii} = 0$. equation (1) has no fixed points for $I_i > 0$. Since any solution of the equation tends to infinity in a finite time, a nonlinear transformation to new variables θ_i may be made [10]: $x_i = \tan\theta_i/2$ which maps the real line onto a circle, and so avoids this blow-up. In terms of the new variables, equation (1) becomes

$$\frac{d\theta_i}{dt} = (1-\cos\theta_i) + (\beta_i + \sum_{j=1}^{N} \alpha_j g_{ji} s_{ji}(\theta_j))(1+\cos\theta_i). \quad (2)$$

The point $\theta = \pi$ represents the point at infinity in equation (1) and is interpreted as firing of a spike; this transformation gives the theta neuron its name.

The dynamics of the synapse $s_{ji}(t)$ follow from the differential equation considered in [11–13]:

$$\frac{ds_{ji}}{dt} = -\frac{s_{ji}}{\tau_{ji}} + e^{-\eta(1+\cos\theta_j)}\frac{1-s_{ji}}{\tau_R}. \quad (3)$$

The synaptic decay time has been denoted by τ_{ji} and τ_R denotes the synaptic rise time.

It is clear from equation (2) that the activity of the ith neuron is regulated by feedback from s_{ji} because s_{ji} depends upon θ_j which in turn depends upon θ_i $(j \neq i)$ through the coupling term having $s_{ij}(\theta_i)$. The coupled system under study is depicted in Figure 1.

Since the time dependence of the bifurcation parameter I_i is brought about because of the feedback $\sum_{j=1}^{N} \alpha_j g_{ji} s_{ji}$ from the other neurons received through the synapse, we chose in this study to keep the external input β_i constant throughout so that the dynamics governing the feedback could be understood better.

3 Coupled theta neurons in the presence of weak noise

At the cellular scale, the activity of real neurons can be influenced by a number of other factors: physical as well as biochemical, and also by random influences: for instance, fluctuations in the neurotransmitter levels at synapses, conductance fluctuations in ion channels or thermal fluctuations [16]. It is therefore of great importance to study the influence of random noise on coupled neuronal dynamics. In this work we have used Gaussian white noise $\xi(t)$ to model these random influences on the dynamics of the coupled generic neurons in equation (2). We consider neurons which are coupled bidirectionally as shown in Figure 1 and subject to Gaussian white noise $\xi(t)$ with the following properties: $\langle\xi(t)\rangle = 0$, $\langle\xi(t)\xi(t')\rangle = 2\sigma\delta(t-t')$. The stochastic variables are taken to obey Stratonovich calculus. Addition of Gaussian white noise ξ to equation (1), manifests as multiplicative noise in equation (2) because of the change of variables to θ, so that the equations now take the form

$$\frac{d\theta_i}{dt} = (1-\cos\theta_i) + (\beta_i + \sum_{j=1}^{N} \alpha_j g_{ji} s_{ji}(\theta_j) + \xi(t))(1+\cos\theta_i). \quad (4)$$

We consider the neuronal output to be described by the variable $u_i = (1-\cos\theta_i)/2$ (as in [14]) since its time series resembles that of the membrane potential in real neurons. This transformation maps the resting point $x_i = 0$ corresponding to $\theta_i = 0$ to $u_i = 0$, and the spiking point $\theta_i = \pi$ to $u_i = 1$ via the relation $u_i = x_i^2/(1+x_i^2)$. This choice of variables enables us to get some new insights into the dynamics underlying the onset of complete synchronization. Equations (4) and (3) then become

$$\dot{u}_i = 2\Big(u_i + (\beta_i + \sum_{j=1}^{N} \alpha_j g_{ji} s_{ji} + \xi)(1-u_i)\Big)\sqrt{u_i(1-u_i)} \quad (5)$$

$$\dot{s}_{ji} = -\frac{s_{ji}}{\tau_{ji}} + \exp\left(-2\eta(1-u_j)\right)\frac{(1-s_{ji})}{\tau_R}. \quad (6)$$

Among the different kinds of synchronous phenomena, we find CS most interesting because the trajectories of the mutually synchronizing systems become identical. The literature contains several papers on CS in different coupled systems; however systems with more complicated couplings, such as that described by equations (5) and (6) have not been intensively studied yet – an adequately satisfying explanation of conditions and circumstances under which CS can occur in such systems is still lacking.

Noise-induced CS in systems through common additive white noise was studied in [21] who showed that the existence of a significant contraction region in phase space was a necessary condition for occurrence of CS – the systems studied in their work were the Lorenz and Rossler systems – far easier to handle analytically in comparison to our system.

For type-I neurons, we could expect CS among neurons through common noise alone, because of the existence of a contraction region close to the stable manifold of the saddle. When any two type-I neurons are coupled together as in equations (5, 6), then the nature of the eigenvalues

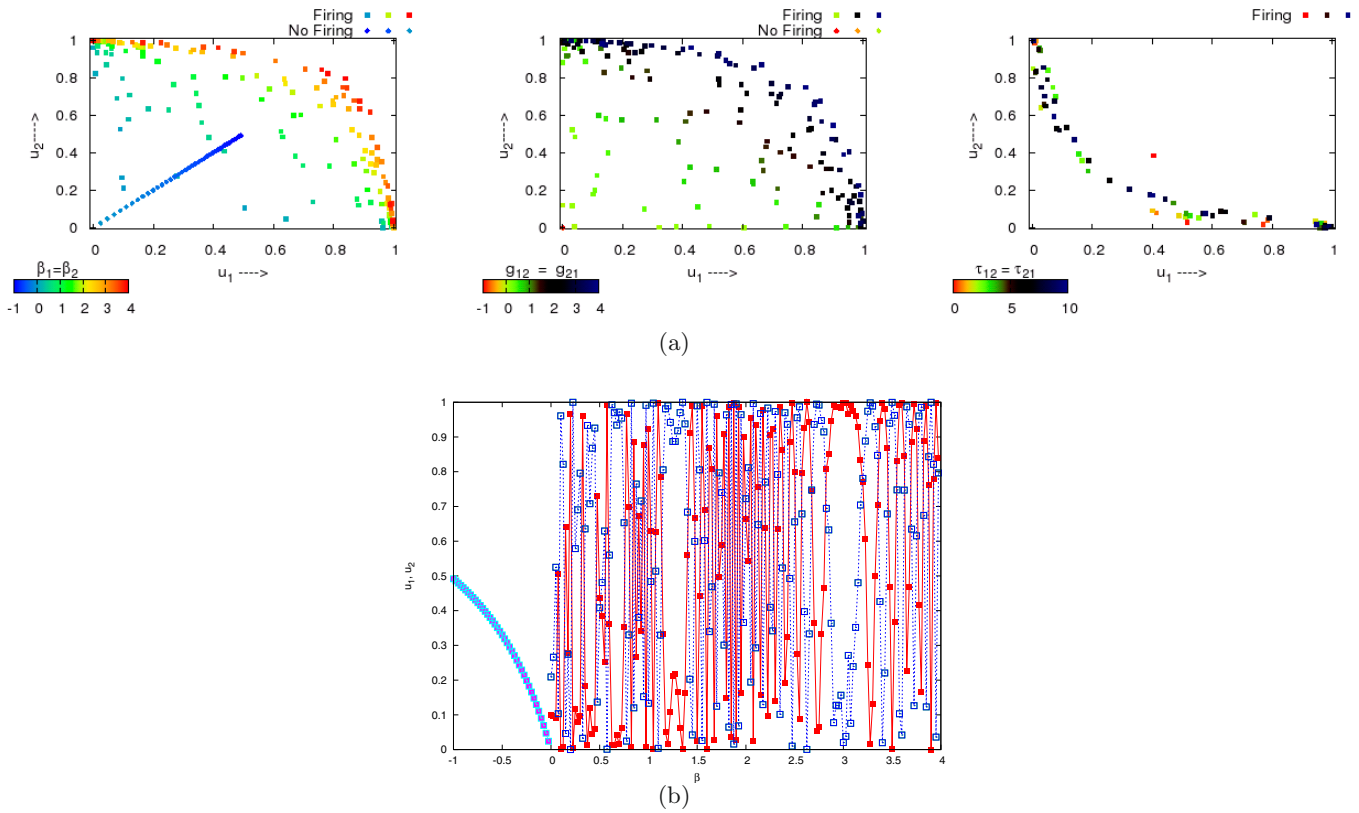

Fig. 2. (Color online) (a) Activity diagrams for EE coupling: effect of different parameters on firing: left: changing input $\beta_1 = \beta_2 = \beta$, middle: changing coupling strength $g_{12} = g_{21} = g$, right: changing synaptic decay time $\tau_{12} = \tau_{21} = \tau$. (b) Plot in (a, left) depicted in a more standard way, as variation of neuron outputs (on the y-axes) with the input β (on the x-axis) showing bifurcation in the neuron activity. Blue and red points ($\beta > 0$) correspond to "firing" neurons of (a), with cyan and magenta (overlapping) points ($\beta < 0$) correspond to "non-firing" neurons.

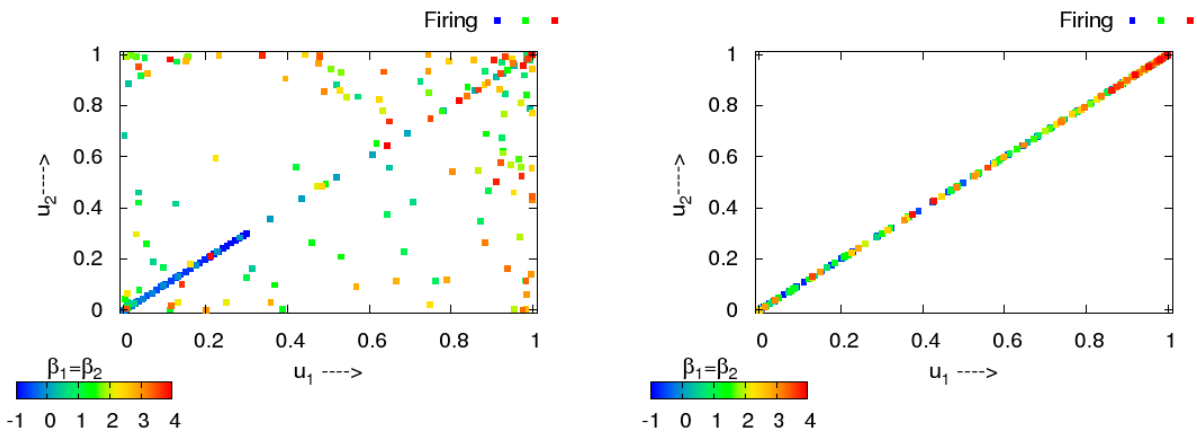

Fig. 3. (Color online) Complete synchronization in EE system in the presence of noise: left: $\sigma = 0.375$, right: $\sigma = 1.0$.

of the stability matrix of the coupled system at the fixed points would determine whether such a contraction region could exist, and if so, its nature.

However, for our system in equations (5, 6), linear stability analysis fails as the Jacobian becomes singular at the fixed points. Physically, this is a reflection of neuronal spiking with the inbuilt phase-resetting mechanism contained in equation (3). Moreover, the time dependence of the control parameter and its continuous dependence upon the feedback also makes an analytical approach non-straightforward. We therefore perform some numerical and computer-based studies which provide some useful insights on the coupled dynamics.

Just as in [21], we define CS to take place between neurons 1 and 2 on obtaining a vanishing value for the

quantity $\langle |u_1 - u_2| \rangle$ which is the synchronization error averaged over all iterations.

It is well known that inhibitory couplings help in producing phase-synchronous activity in deterministic systems [9–11]. For the system under study in Figure 1 too, we found that antiphase states are stable in the noiseless situation for EE synapses: these states become completely in-phase in the presence of noise. This does not happen in general for IE synapses [10,15].

In the uncoupled system neuronal firing starts after the threshold value $\beta = 0$ is crossed. In the coupled system under study (Fig. 1), the picture changes and the input I_i acquires time dependence; neuronal firing is then controlled by the different parameters in equations (2) and (3): the coupling strength $\alpha_j g_{ji}$, the decay time of the synapse τ_{ji}, the external input β_i, etc.

We proceed as follows in our investigation. We look at the behaviour of the neuronal output variables u_1, u_2 for different parameters in the system in the noiseless case. The addition of noise changes the behaviour, introducing order into the system. However, the outcome is different for the EE and IE cases. To avoid any confusion, we therefore detail our results separately, for EE and IE, respectively, in the coming subsections. A fruitful way of understanding the physics of any system is to make an analogy with a more common, familiar one. Rewriting equations (5) and (6) enables a resemblance of the coupled neurons to a nonlinear anharmonic oscillator to be observed, to help understand its behaviour. We do this below.

4 EE synaptic coupling

In Figure 2, we depict for EE coupling, the variations of both the neuronal output variables u_1 and u_2 with the different parameters in the system for the noiseless case: the constant inputs $\beta_1 = \beta_2$, the coupling strengths $g_{12} = g_{21}$, and the synaptic decay time τ_{ij}, varying one at a time and keeping the other two fixed. These portrayals of the system's behaviour with changing parameters have been done differently, with the colour coding showing the varying values of the control parameter. The advantage of plotting them this way is essentially to portray the maximum possible information (for instance variation of both neuronal variables simultaneously) at a glance. The diagram distinguishes between states where both neurons are active and evolving ("firing" in this context implying that there is a difference between consecutive outputs for both neuron 1 and neuron 2), and states where one or both neurons are quiescent or have reached a steady (unchanging) state ("non-firing") implying that there is no difference between consecutive outputs of one or both neurons). Thus the following states would be classified as "firing" in the plot: $|u_1(t+1) - u_1(t)| > 0$ and $|u_2(t+1) - u_2(t)| > 0$ while the following would be classified as "non-firing":

(i) $|u_i(t+1) - u_i(t)| = 0$ and $|u_j(t+1) - u_j(t)| > 0$, $i \neq j$;
(ii) $|u_i(t+1) - u_i(t)| = 0$ and $|u_j(t+1) - u_j(t)| = 0$, $i \neq j$.

Thus, even the state where $u_1(t+1) = 1$, $u_1(t) = 1$, with $|u_2(t+1) - u_2(t)| \geq 0$, i.e., where neuron 1 has reached its peak value of 1 in consecutive firings, while the other neuron may have likewise peaked or have shown some or no change, we would classify it under the "non-firing" plot. Thus, it would be most appropriate to term these plots "Activity Diagrams", indicative of the state of active evolution for both neurons in the coupled system.

In the noiseless case the neurons can be excitable and fire only if the inputs β_i are above the threshold $\beta_i = 0$. For $\beta_i < 0$, there are stable and unstable fixed points, but no periodic firing can arise as they are below the threshold. The maximal value of unity for u_i corresponds to the generation of the spike (peak value).

In Figure 2a, we observe in the first plot where $\beta_1 = \beta_2$ is the varying parameter for fixed g_{ij} and τ_{ij}, that above the firing threshold $\beta > 0$, the points in the plot for any β trace out a quadrant of a circle – this is especially apparent for large β, ($\beta \approx 4$): this is a reflection of the stability of the antiphase states u_1 and u_2 in the EE case. In the adjacent (middle) plot where $g_{ij} = g_{ji}$ is the control parameter, all the points plotted are the square "firing" ones because the input has been chosen in this case to be $\beta_1 = \beta_2 = 0.1 > 0$. Here again it was seen that the solutions u_1 and u_2 are out of phase and the points trace out a roughly circular curve: the last plot in Figure 2a where the decay time $\tau_{ij} = \tau_{ji}$ of the gating variable is the parameter shows that the magnitudes of u_1 and u_2 do not show appreciable change with change in magnitude of τ_{ij}.

To make the plots clearer, we have plotted the variation of both neurons u_i with β in the standard manner, in Figure 2b. For $\beta < 0$ the neurons do not fire and each solution is non-oscillatory; after the threshold is crossed however, i.e., for $\beta > 0$, both neurons show oscillatory behaviour – the plot therefore shows bifurcation of neural activity. We observe that u_1 and u_2 oscillate out of phase with each other.

In Figure 3 we show the development of noise-induced synchrony as the noise strength is increased from 0.375 (left) to 1.0 (right) for EE coupling: a drastic change in the firing activity pattern is observed on introduction of weak noise: in contrast to Figure 2, all neurons now fire. Even for negative values of β_1 and β_2 (corresponding to stable points in the flow of the uncoupled system: the neurons do not fire in the deterministic system), addition of weak noise induces firing by raising total input levels to threshold values. One observes that the nearly symmetrical distribution of points on either side of the diagonal $u_1 - u_2 = 0$ in (Figs. 2a) in the noiseless case, converges towards the diagonal in the presence of noise. As the noise strength is increased, the firing of the two neurons is completely synchronized and for $\sigma = 1.0$, all the points line up along the diagonal and are CS solutions.

4.1 Analogy to a mechanical system

We can get some insight into the dynamics underlying the development of CS in the EE systems by drawing an

analogy with a mechanical system. To do this, we rewrite equations (5, 6) for $N = 2$, $\alpha_1 = 1$, $\alpha_2 = 1$ as:

$$\begin{aligned}
\dot{u}_1 &= f_D(u_1) + \beta_1 f_n(u_1) + g_{21}(s_{21}+1)(u_2) f_n(u_1) \\
&\quad + \xi f_n(u_1) \\
\dot{u}_2 &= f_D(u_2) + \beta_2 f_n(u_2) + g_{12}(s_{12}+1)(u_1) f_n(u_2) \\
&\quad + \xi f_n(u_2) \\
&\ddot{s}_{21} + h(u_2)\dot{s}_{21} + (\Phi(u_2) + \Psi(u_2) g_{12}(s_{12}+1)) s_{21} = \\
&\quad - \Psi(u_2) s_{21} \xi(t) \\
&\ddot{s}_{12} + h(u_1)\dot{s}_{12} + (\Phi(u_1) + \Psi(u_1) g_{21}(s_{21}+1)) s_{12} = \\
&\quad - \Psi(u_1) s_{12} \xi(t)
\end{aligned} \tag{7}$$

where

$$f_D(u_i) = 2u_i^{3/2}(1-u_i)^{1/2};\ f_n(u_i) = 2u_i^{1/2}(1-u_i)^{3/2};$$
$$h(u_i) = \left(\frac{1}{\tau_{ij}} + \frac{e^{-2\eta(1-u_i)}}{\tau_R}\right);$$

$$\begin{aligned}
\Phi(u_i) &= 2\eta \frac{e^{-2\eta(1-u_i)}}{\tau_R}(f_D(u_i) + \beta_i f_n(u_i)); \\
\Psi(u_i) &= 2\eta \frac{e^{-2\eta(1-u_i)}}{\tau_R} f_n(u_i)
\end{aligned} \tag{8}$$

and where a shift of s_{ij} by unity has been performed in equations (7) (and later on in Eq. (14)) for the sake of putting these in the more convenient form displayed. As can be seen, these equations are not easily amenable to a quick analysis of the physics that they describe. The equations for the gating variables s_{ij} in equations (7) resemble those of a nonlinear anharmonic oscillator with a nonlinear damping term and a nonlinear restoring force term with variable spring coefficient $(\Phi(u_i) \pm \Psi(u_i) g_{ji}(s_{ji}+1))$, with the plus sign for excitatory couplings and minus sign for inhibitory couplings. In the EE system, the variable spring coefficient is $(\Phi(u_i) + \Psi(u_i) g_{ji} s_{ji})$ for both s_{21} and s_{12} and it is like a system of two damped (nonlinear) spring-mass systems coupled together, with both "springs" getting extended or both getting compressed (though by different amounts) at the same time. This, coupled with the same (plus) sign in the u_i equations lead to both neurons eventually firing at the same rate if the neurons happen to be identical.

The addition of common weak noise $\xi(t)$ to both neurons (Eq. (5)) changes the potential at the synapses (in mechanistic terms, it affects the "stiffness" of the synaptic conductances in Eq. (7)), and also modulates the firing thresholds of u_1 and u_2 by injecting energy at random points in time.

For EE coupling, the thresholds of each neuron is modulated similar to the other due to the common noise and if the noise strength is adequate, neuronal firing eventually occurs in synchrony.

4.2 Variation of instantaneous frequency with instantaneous phase of neuronal inputs

To understand how this CS actually comes about, in [15] we constructed the analytical signal $B_i(t)e^{i\rho_i(t)} = I_i(t) + iH(I_i(t))$ for the inputs I_i and those for the neuron outputs u_i: $w_i(t) = u_i(t) + H(u_i(t)) = R_i(t)e^{i\phi_i(t)}$ using Hilbert transforms and showed that the instantaneous amplitudes B_i and instantaneous phases ρ_i of the inputs evolve in time according to:

$$\begin{aligned}
\dot{B}_i(t) &= -B_i\left(\frac{1}{\tau_{ji}} + \frac{e^{-2\eta(1-R_j\cos\phi_j)}}{\tau_R}\cos(2\eta R_j \sin\phi_j)\right) \\
&\quad + \frac{\beta_i}{\tau_{ji}}\cos\rho_i + \frac{1}{\tau_R}\left(\beta_i + \sum_j \frac{\alpha_j g_{ji}}{\tau_R}\right)\cos((2\eta R_j \sin\phi_j) \\
&\quad - \rho_i)\ e^{-2\eta(1-R_j\cos\phi_j)} \\
\dot{\rho}_i(t) &= -\frac{e^{-2\eta(1-R_j\cos\phi_j)}}{\tau_R}\sin(2\eta R_j\sin\phi_j) - \frac{\beta_i}{B_i\tau_{ji}}\sin\rho_i \\
&\quad + \frac{1}{\tau_R B_i}\left(\beta_i + \sum_j \frac{\alpha_j g_{ji}}{\tau_R}\right)\sin((2\eta R_j\sin\phi_j) \\
&\quad - \rho_i)\ e^{-2\eta(1-R_j\cos\phi_j)}.
\end{aligned} \tag{9}$$

We argued in [15] that CS is achieved if the rate of change of *instantaneous* frequency ($\dot{\phi}$) with the *instantaneous* phase (ϕ) of the input for neuron 1 matches exactly that for neuron 2. This is not a trivial statement since the system incorporates feedback as well as noise.

This matching of values happens because noise produces delay in the decay time of the synaptic gating variables, causing CS to eventually occur. In Figure 4a we demonstrate this through a sequence of time series of s_{ij} for increasing noise strengths. We find that addition of weak noise delays the decay time of s_{ij} gradually, eventually lowering its minimum to zero. This produces a delay in the onset of the next s_{ij} peaks which in turn delays the input I_i to the post-synaptic neuron at a future time instant. The decay time of s_{ij} is increased further as the noise strength is increased. The periodically occurring maximal values of the inputs then arrive at the post-synaptic neurons later than in the previous cases and this gets reflected in the firing pattern of neurons as departures from the noiseless/previous values of the differences $(u_1 - u_2)$ and those of the phase differences between the neurons. This can be seen more clearly in Figure 4b where the synaptic conductance for a single neuron is shown for increasing noise strengths.

For a given set of β, τ_{ij}, η, τ_R, the values of the instantaneous phases ϕ_i and those of their temporal variation, i.e., the instantaneous frequencies, are determined by the synaptic coupling strengths $\alpha_{ij}g_{ij}$ and the noise strength, which are inputs received at the synapse. When the variation of the instantaneous values with instantaneous phases of the *inputs* to neuron 1 matches with that for neuron 2, then it is reasonable to expect CS to occur in the EE system, because the instantaneous values ϕ_1 and $\dot{\phi}_1$ of neuron

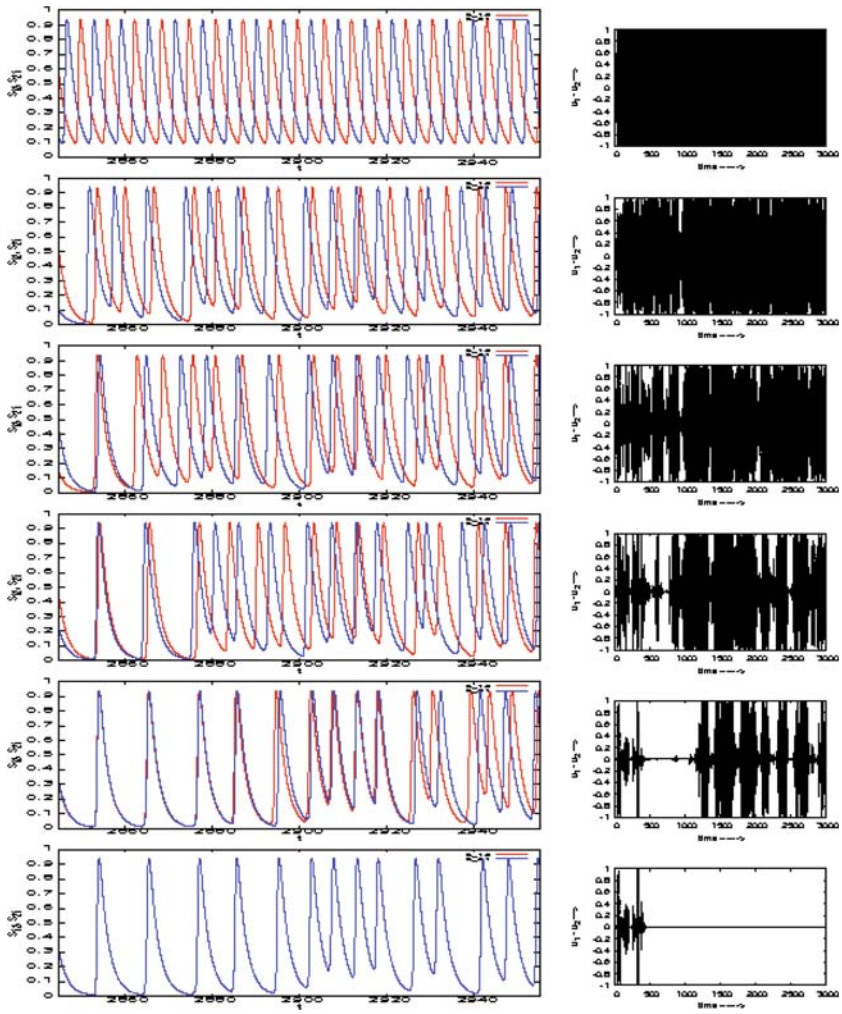

(a)

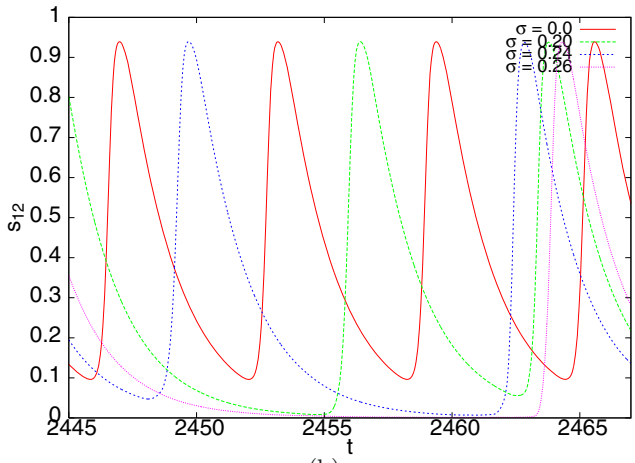

(b)

Fig. 4. (Color online) Noise produces delay in the decay time of the synaptic gating variables which eventually bring about CS in neurons with EE coupling. These plots illustrate this. (a) Plots at the left are time-series of the synaptic conductances s_{12} (in red) and s_{21} (blue) and the corresponding differences of the neuronal outputs $(u_1 - u_2)$ are shown at the right for EE coupling. These plots show the approach to CS as σ is increased from top to bottom: $\sigma = 0$, $\sigma = 0.20$, $\sigma = 0.24$, $\sigma = 0.26$, $\sigma = 0.29002$, $\sigma = 0.2900200338$. (b) Detail of the plots on the left in (a) above are shown for increasing noise strengths $(\sigma = 0.0, 0.20, 0.24, 0.26)$ for a single synaptic gating variable s_{12}.

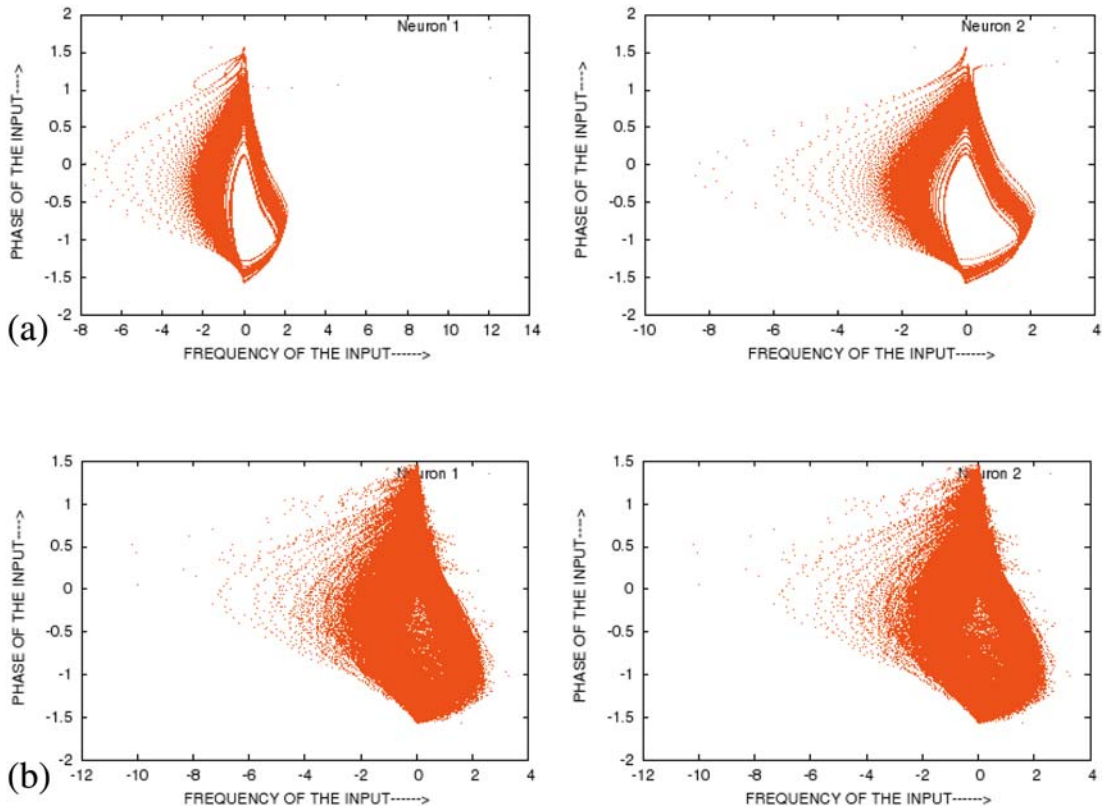

Fig. 5. (Color online) Instantaneous frequency vs instantaneous phase of inputs to neurons ("flame plots") for EE coupling for: (a) $\sigma = 0.0$; (b) $\sigma = 0.75$. Parameters used are: $\beta_1 = 0.0$, $\beta_2 = 0.00001$, $g_{12} = g_{21} = 0.3$, $\tau_{12} = \tau 21 = 2.0, \tau_R = 0.1, \eta = 5.0$. (Initial conditions: $\theta_1 = 0.0, \theta_2 = 0.0, s_{12} = 0.0, s_{21} = 0.0$) – Noise-induced CS occurs.

1 change in step with ϕ_2 and $\dot{\phi}_2$ respectively of neuron 2. This forces the amplitudes of neurons 1 and 2 to become identically the same, because if they do not, then both conditions $\phi_1 = \phi_2$ and $\dot{\phi}_1 = \dot{\phi}_2$ cannot simultaneously be maintained. Such a plot (instantaneous frequency $\dot{\phi}$ versus instantaneous phase ϕ) of the *input* to each neuron then has a characteristic flame shape (Fig. 5), which exactly matches with that for the other neuron when CS occurs [15], and this identity of the plots can be used as an indicator of CS. In this plot we have used slightly different values for the inputs β_1 and β_2. This small difference in the input values makes the systems non-identical since neuron 2 receives a very small non-zero constant input. The plot shows that noise-induced CS occurs for coupled non-identical systems also when the instantaneous "flame plots" of the neuronal inputs are identical.

4.3 Input-frequency curves and Lyapunov exponents

The input-firing frequency curves for the coupled system plotted in Figure 6 for different values of the coupling strength are typical characterizations of type-I neurons, differing from them only in that, even at $\beta_i = 0.0$ there is a non-zero frequency of neuronal firing, since $I_i \neq 0$. Lyapunov exponents have been calculated and shown alongside.

These frequency-input curves indicate firing via a saddle-node bifurcation for the coupled EE system. Since the occurrence of a saddle-node bifurcation allows for a contraction region along and close to the stable manifold of the saddle, and in conformity with the result of [21], it seems reasonable to expect CS to occur among systems coupled through EE synapses.

Figure 6a depicts identical neurons with EE coupling ($g_{ij} = g_{ji} = 0.3$ and other parameters as shown): the system is periodic with the presence of only a single frequency. Increasing the coupling strength of one neuron to $g_{ji} = 0.45$, all other parameters and conditions remaining as before (corresponding to non-identical neurons with EE coupling) produces a second frequency after β_i crosses a value of approximately 0.7 (Fig. 6b). This is manifested in the Lyapunov exponent curve: the second largest Lyapunov exponent also becomes zero at the same point, indicating the presence of a second frequency in the system. As this transition from a periodic to a quasiperiodic state involves variation in g_{ji} and β_i, for given τ_{ij}, τ_R, a codimension two bifurcation is indicated at this point.

4.4 Noise-induced variation of firing frequency

Largest Lyapunov exponents in the presence of noise were calculated in [15] using the stochastic Runge-Kutta-4 method. We found that in both EE and IE cases, the

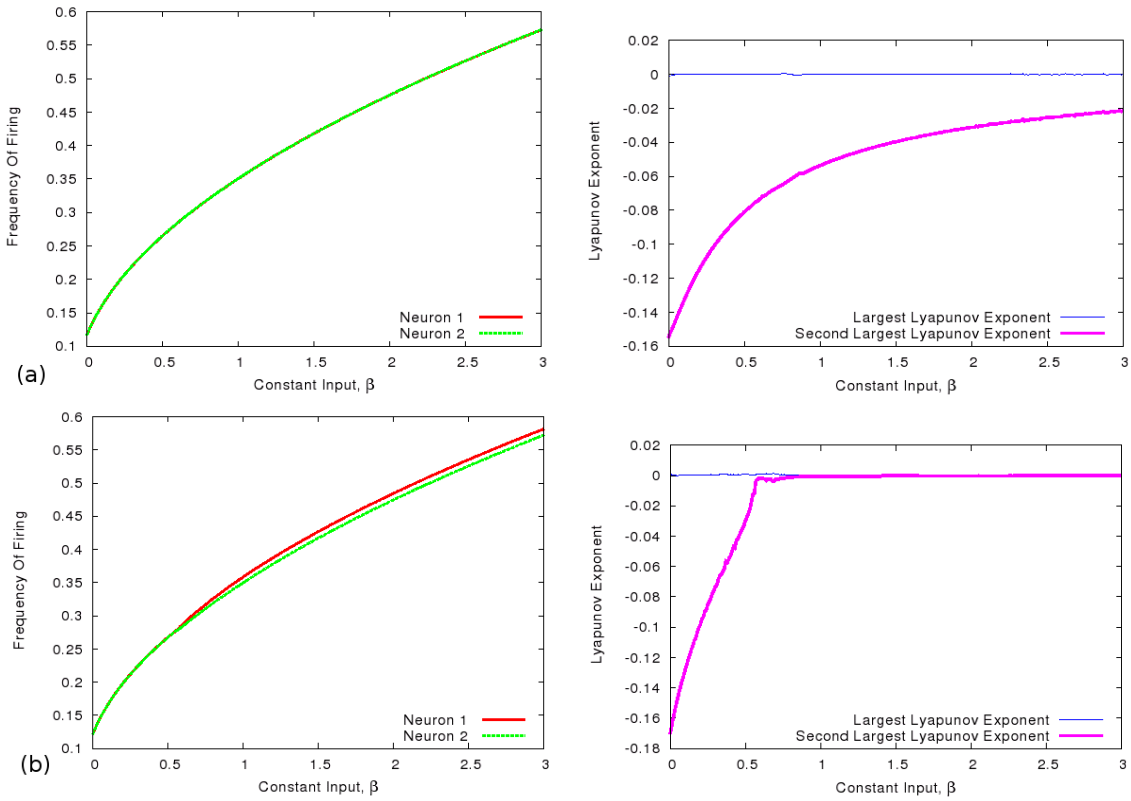

Fig. 6. (Color online) Firing frequency and Lyapunov exponents versus input curves for EE coupling, for $\tau_{12} = \tau_{21} = 2.0, \eta = 5.0, \tau_R = 0.1$, $\sigma = 0$: (a) $g_{12} = g_{21} = 0.3$; (b) $g_{12} = 0.3$, $g_{21} = 0.45$.

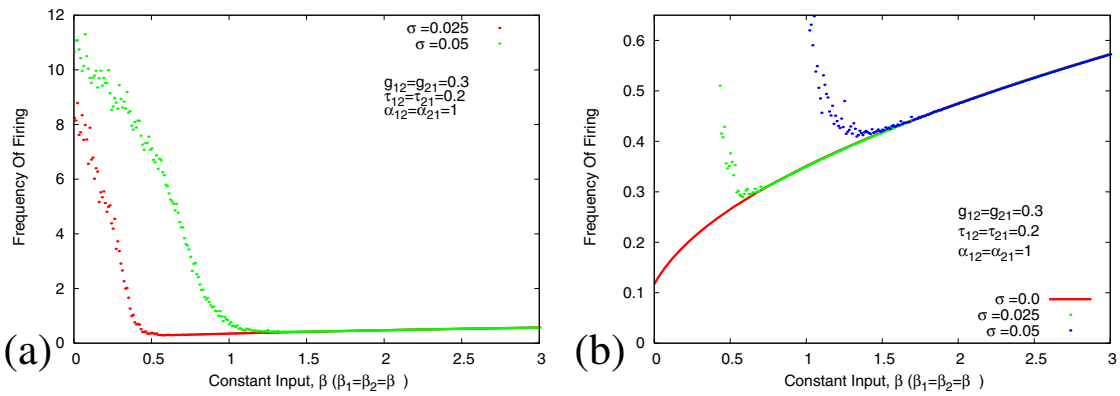

Fig. 7. (Color online) Frequency of firing and effect of noise on it for EE coupling for: (a) $\sigma = 0.025$ and $\sigma = 0.05$, (b) curves of the left graph plotted alongside values for $\sigma = 0$.

largest Lyapunov exponent λ_1 becomes more negative on the addition of noise demonstrating the role of noise in bringing about order into the system.

In the presence of weak noise, firing frequency changes with β_i differently for the excitatory and the inhibitory neurons, depending upon whether the coupling is of EE or IE type. For EE coupling, this is displayed in Figure 7 and the plots for the noiseless case is shown in red in Figure 7b.

One observes that the frequency of firing of both excitatory neurons starts from a large non-zero value even at $\beta_1 = \beta_2 = 0$ (Fig. 7). As β_i is increased further, the frequency decreases rapidly, and after a certain value of β_i, the curve merges with that for $\sigma = 0$, taking on the very same frequency values as for the noiseless case, so that from this point onwards, the frequency once again increases with increase of β_i, but the increase is now gradual.

4.5 Noise-induced synchronization and locking to partially synchronized state

Numerous studies on CS in coupled systems have been previously reported in other systems (see for

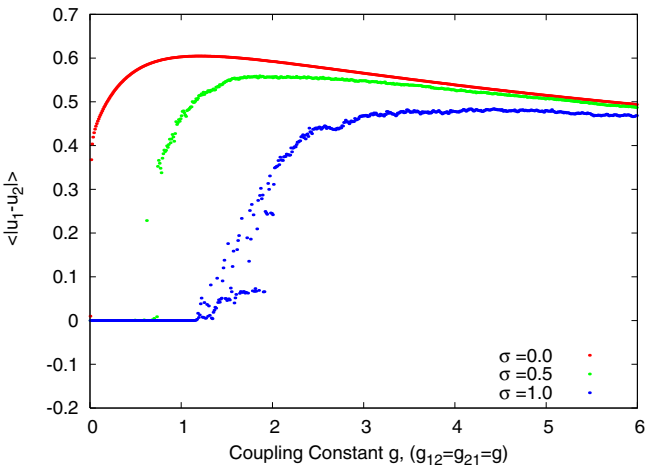

Fig. 8. (Color online) Variation of $\langle|u_1-u_2|\rangle$ with the coupling strength $g_{12}=g_{21}=g$ for EE coupling. Parameter values are: $\tau_{12}=\tau_{21}=2.0, \beta_1=\beta_2=0.1, \tau_R=0.1$ (initial conditions: $\theta_1=0.0, \theta_2=0.01, s_{12}=0.0, s_{21}=0.0$).

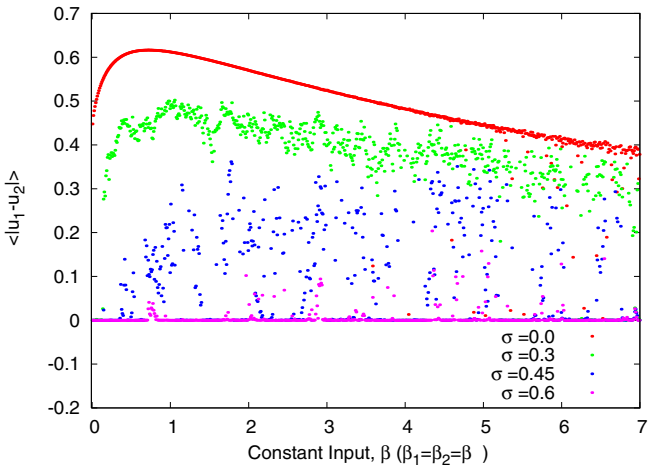

Fig. 9. (Color online) Variation of $\langle|u_1-u_2|\rangle$ with the input β for EE coupling: parameter values are: $\tau_{12}=\tau_{21}=2.0$, $g_{12}=g_{21}=0.3, \tau_R=0.1$. (Initial conditions: $\theta_1=0.0, \theta_2=0.01, s_{12}=0.0, s_{21}=0.0$).

instance [4–6,19–22] and references therein). Noise-induced CS in coupled theta neurons happens for EE coupling in a certain parameter range. However, we have not yet succeeded in observing it for IE coupling in a system of just two neurons. There appears to be definite relations between the magnitude of the output-difference between the two neurons averaged over all iterations $\langle|u_1-u_2|\rangle$, and the various parameters of the theory such as g_{ij}, β_i, and the noise strength σ, for both EE & IE couplings, and these may be quantified by plotting these quantities (Figs. 8–13).

In Figure 8, $\langle|u_1-u_2|\rangle$ is plotted as a function of g_{ij} for $\beta_1=\beta_2=0.1$ in the case of EE coupling. It is seen that increasing the noise strength helps in bringing about synchronization for low values of g_{ij}. At higher coupling strengths, CS is destroyed as $\langle|u_1-u_2|\rangle$ increases steadily, but then it plateaus off, approaching a limiting value of approximately 0.5 at about $g_{ij}=6$ for all noise strengths. Partial synchronization therefore takes place as the system gets locked to this state.

In [15] we found for EE synapses that for a given input, the critical coupling strength g_c before which the neurons are completely synchronized, and beyond which they are desynchronized depends upon the noise strength as:

$$g_c \sim a\sigma^{1/2} \tag{10}$$

where for the choice of parameters we had considered, we had $a \approx 1.1$. In that work, we also found for curves such as those in Figure 8, the following functional dependence of the synchronization error on g for the entire regime of coupling strengths after the onset of desynchronization:

$$\langle|u_1-u_2|\rangle \sim a(\sigma)-b(\sigma)-\frac{g_c^4}{g^3} \tag{11}$$

where the constants a and b are noise-dependent.

The variation of $\langle|u_1-u_2|\rangle$ with β_i for EE synapses can be seen in Figure 9. CS does not happen for $\sigma=0$, but increasing noise strength decreases the difference. At lower nonzero noise strengths, the system oscillates between the completely synchronized and the unsynchronized states. At a moderate noise strength of $\sigma=0.6$, the system shows CS for nearly the entire range of β_i shown in the figure.

In Figure 10, we show the variation of $\langle|u_1-u_2|\rangle$ with noise strength at different g_{ij} values, for $\beta_i=0.1$. We find that in neurons coupled through EE synapses, the transition to CS occurs at larger noise strengths for stronger coupling strengths; for weaker couplings, smaller noise strengths suffice for CS to occur. The system makes large oscillations between two metastable unsynchronized states before settling into the stable synchronized state. We find from an analysis of the plot in Figure 10 that the point where desynchronization gives way to synchronization, i.e., $\langle|u_1-u_2|\rangle \to 0$ begins to be approached, can be given by the relation

$$\sigma_{turn} \approx 0.5\ g^{3/4}+\beta. \tag{12}$$

We find that the maximum value that $\langle|u_1-u_2|\rangle$ takes is at minimal noise strength σ and is related to the coupling strength g (for $\beta=0.1$) by

$$\langle|u_1-u_2|\rangle_{max} \approx 0.607\ g^{0.1}. \tag{13}$$

This relation is made clear from the plot in Figure 10c.

We now discuss our results for neurons coupled through IE synapses.

5 IE synaptic coupling

In Figure 11a we depict, as for the EE case, variations of both neuronal variables u_1 and u_2 simultaneously, with β, g_{ij} and τ_{ij}, in the absence of noise where the out of phase solutions are not the stable ones. The "firing" (active) points are more randomly distributed in this case.

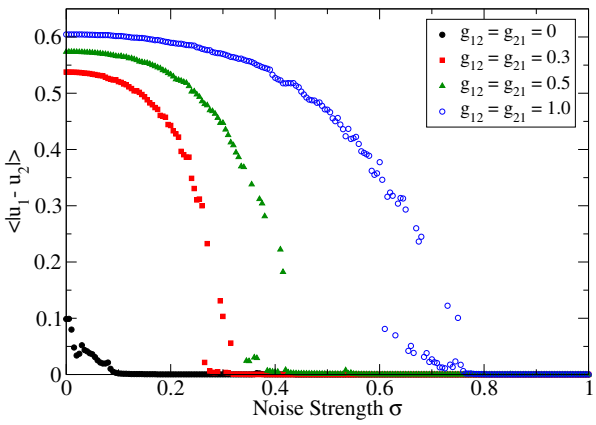

(a)

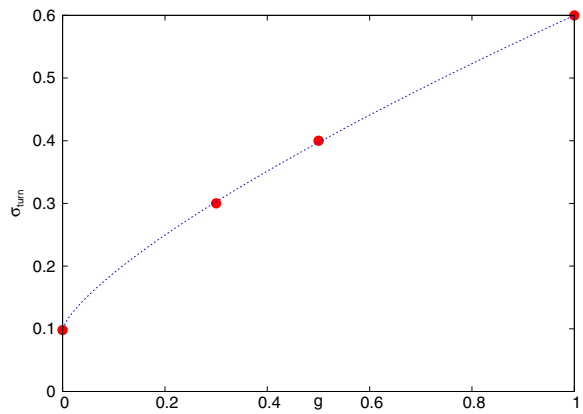

(b)

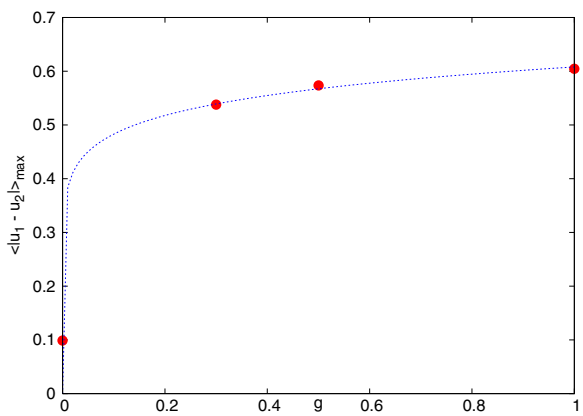

(c)

Fig. 10. (Color online) (a) Variation of $\langle|u_1 - u_2|\rangle$ with the noise-strength σ for EE coupling. (b) critical noise strength as a function of g (Eq. (12)); (c) $\langle|u_1 - u_2|\rangle_{max}$ versus g (Eq. (13)). parameter values are: $\beta_1 = \beta_2 = 0.1, \tau_{12} = \tau_{21} = 2.0, \tau_R = 0.1$. (initial conditions: $\theta_1 = 0.0, \theta_2 = 0.01, s_{12} = 0.0, s_{21} = 0.0$).

In contrast with the EE case, for IE coupling, we observe in Figure 11a that the distribution of the solutions about the diagonal $u_1 - u_2 = 0$ is far from being symmetric. Figure 11b shows the variation of u_i activity with β in a more standard way. The solutions for β less than the threshold value (i.e. for $\beta < 0$) show stable, non-oscillatory behaviour. All u_i for $\beta > 0$ however show large oscillations.

In the presence of noise, the IE system never achieves CS of its solutions. Introduction of weak noise does however bring about some order even in the IE case and this can be visualised in the plots in Figures 12 for noise strengths 0.5 and 1.0, where consecutive points in the u_1-u_2 plane have been connected through a curve. The originally zig-zag trajectories in the noiseless case are now replaced by smooth curves which evolve in time exploring large regions of the phase space for increasing values of β_i in a definite, orderly manner.

5.1 Analogy to a mechanical system

In the case of IE synaptic couplings, addition of even very weak noise greatly affects the neuronal outputs, firing rates and the inputs they receive. For this type of coupling, it is clear from the time series that the inputs have fast and slow branches always, characteristic of relaxation dynamics. In this case, equations (5) and (6) can be rewritten (similar to the EE system) for $N = 2$, and $\alpha_1 = 1, \alpha_2 = -1$, as:

$$\begin{aligned}
\dot{u}_1 &= f_D(u_1) + \beta_1 f_n(u_1) - g_{21}(s_{21}+1)(u_2) f_n(u_1) \\
&\quad + \xi f_n(u_1) \\
\dot{u}_2 &= f_D(u_2) + \beta_2 f_n(u_2) + g_{12}(s_{12}+1)(u_1) f_n(u_2) \\
&\quad + \xi f_n(u_2) \\
\ddot{s}_{21} &\quad + h(u_2)\dot{s}_{21} + (\Phi(u_2) + \Psi(u_2) g_{12}(s_{12}+1)) s_{21} = \\
&\quad - \Psi(u_2) s_{21} \xi(t) \\
\ddot{s}_{12} &+ h(u_1)\dot{s}_{12} + (\Phi(u_1) - \Psi(u_1) g_{21}(s_{21}+1)) s_{12} = \\
&\quad - \Psi(u_1) s_{12} \xi(t)
\end{aligned} \tag{14}$$

here the nonlinear restoring force has variable spring coefficient $(\Phi(u_1) - \Psi(u_1) g_{21}(s_{21}+1))$. This restoring force is incremented for s_{21} but reduces for s_{12}. The system can be visualised crudely as two damped spring-mass systems, one with a very stiff spring and the other with a very loose spring coupled together. The extension of one and simultaneous compression of the other spring leads to separation of time scales and relaxation oscillations of the synaptic conductances (Fig. 13). These are fed as inputs to the neurons, again in the u_2 equation with a plus sign, while in the equation for u_1 with a minus sign. This discordance in the inputs results in non-synchrony of the neuronal outputs, and the excitatory neuron fires at a frequency different from the inhibitory neuron; this mutual difference in firing frequency is maintained even on increasing the common external constant input β: this is discussed further on in Section 5.3. Indeed, a canard solution (Fig. 13b) appears to govern the underlying dynamics.

5.2 Variation of instantaneous frequency with instantaneous phase of neuronal inputs

For IE coupling, though modulation of the firing thresholds by common noise occurs simultaneously for the two

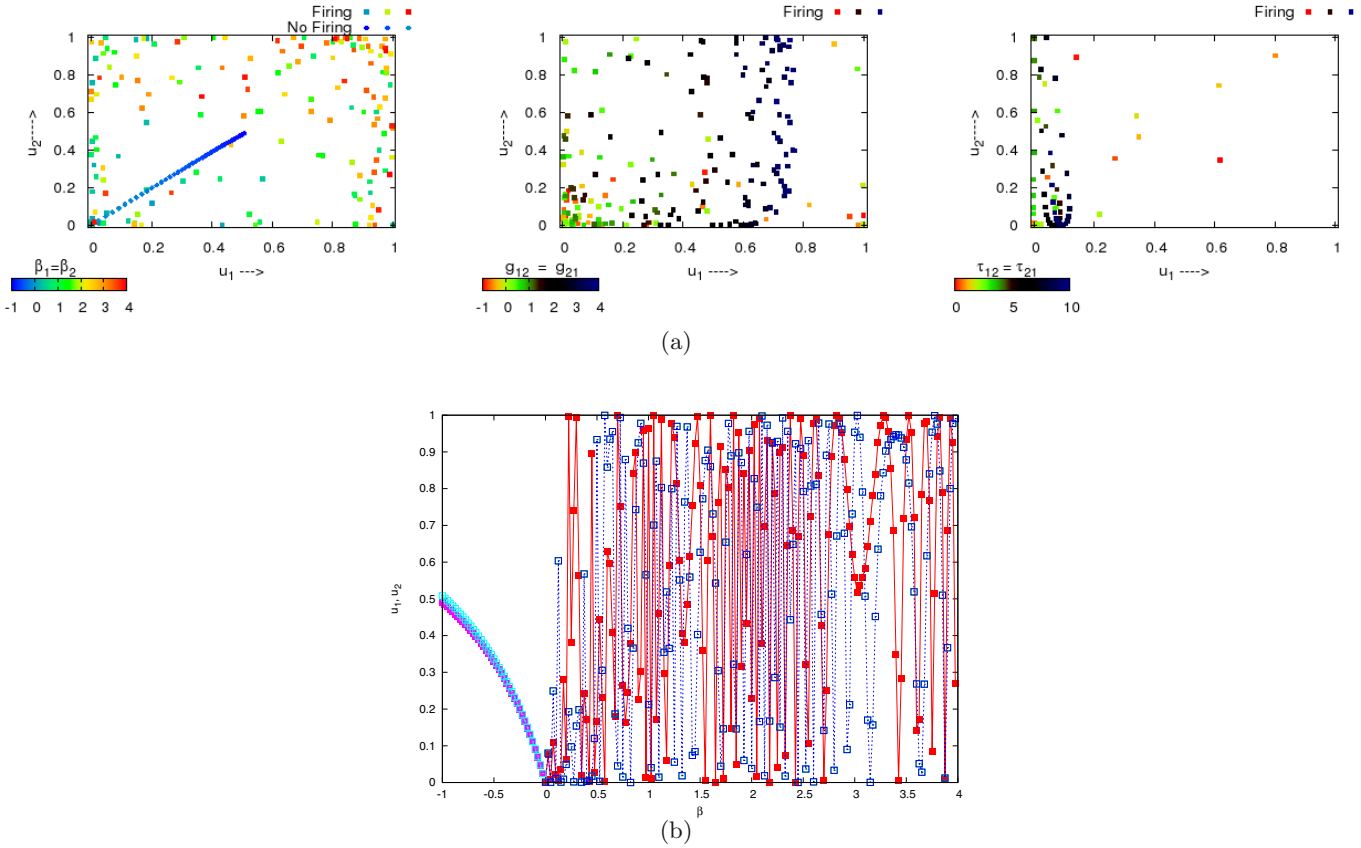

Fig. 11. (Color online) (a) Activity diagrams for IE coupling: effect of different parameters on firing: left: changing input $\beta_1 = \beta_2 = \beta$, middle: changing coupling strength $g_{12} = g_{21} = g$, right: changing synaptic decay time $\tau_{12} = \tau_{21} = \tau$. (b) Plot in (a, left) depicted in the standard way, as variation of neuron outputs (on the y-axes) with the input β (on the x-axis) showing bifurcation in the neuron activity. Blue and red points ($\beta > 0$) correspond to "firing" neurons of (a), with cyan and magenta (overlapping) points ($\beta < 0$) correspond to "non-firing" neurons.

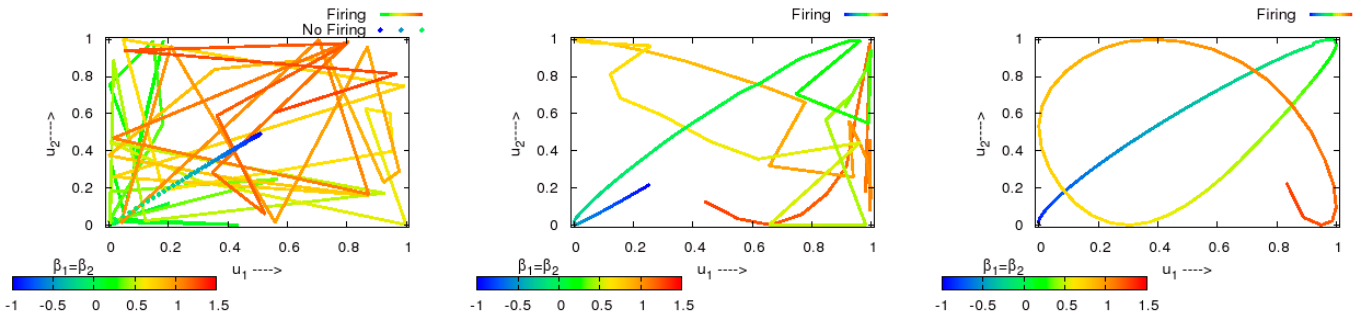

Fig. 12. (Color online) Noise-induced order in IE systems: for (from left to right): $\sigma = 0.0, \sigma = 0.5, \sigma = 1.0$.

neurons, the mutual discordance of the inputs near the firing thresholds because of the opposite signs in the respective coupling terms in equation (14) make it hard for the two neurons to cross the threshold and fire at the same points in time, as we discussed above, using the mechanical analogy with the coupled damped spring-mass systems. Therefore although noise induces order even in IE systems (see Fig. 12), yet complete synchronization becomes very hard to achieve because of the relaxation dynamics of the inputs: the "flame plots" for the two neurons do not match in this case (see Fig. 14 for example).

5.3 Input-frequency curves and Lyapunov exponents

Unlike the EE case, we cannot expect CS in the IE case, because the firing pattern (Fig. 15) does not indicate presence of a saddle for both neurons – the firing frequency

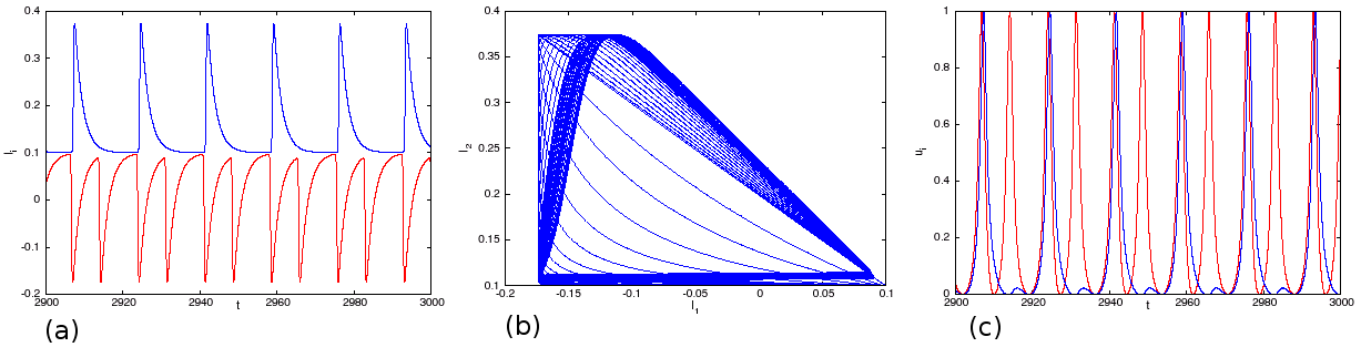

Fig. 13. (Color online) IE system: (a) relaxation oscillations of inputs; (b) canard in the I_1-I_2 plane; (c) time series of neuronal outputs u_i. Here, $g_{12} = g_{21} = 0.3, \tau_{12} = \tau_{21} = 2.0, \tau_R = 0.1, \eta = 5.0, \beta_1 = \beta_2 = 0.1, \alpha_1 = +1, \alpha_2 = -1$.

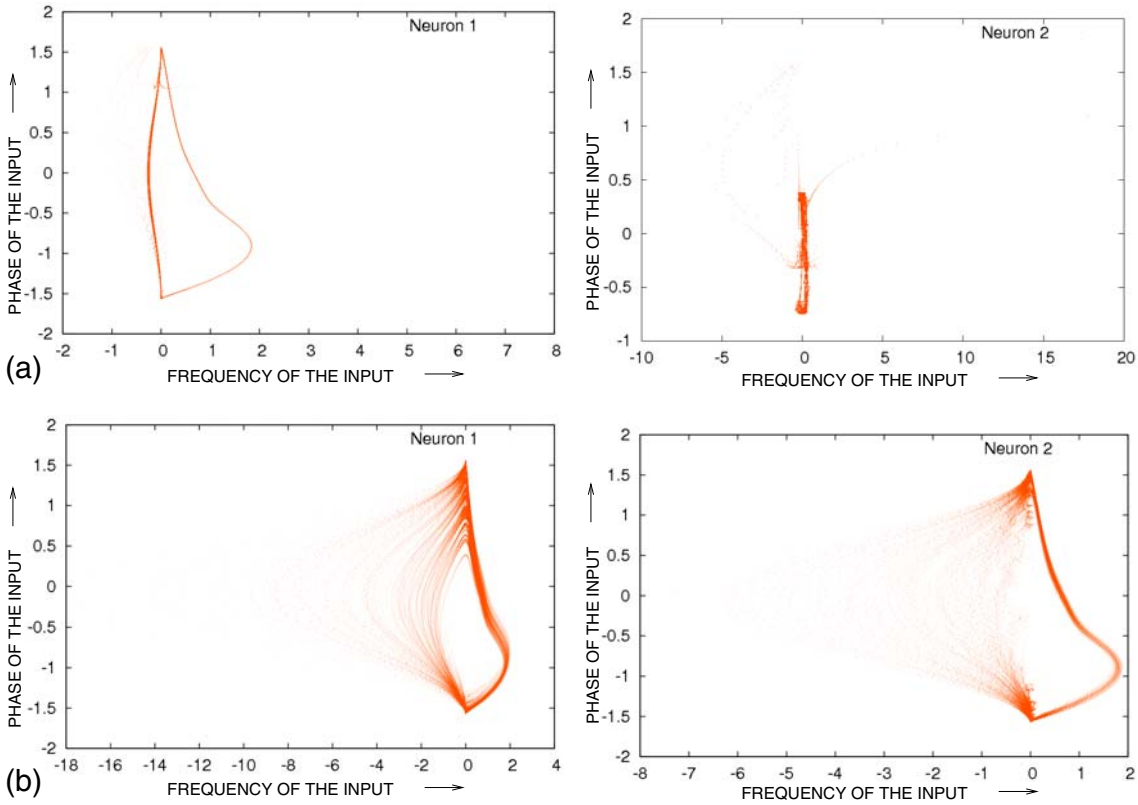

Fig. 14. (Color online) Instantaneous frequency vs instantaneous phase of inputs to neurons ("flame plots") for IE coupling for: (a) $\sigma = 0.0$, $\beta_1 = \beta_2 = 0.1$, $g_{12} = g_{21} = 0.3$, $\tau_{12} = \tau_{21} = 2.0, \tau_R = 0.1, \eta = 5.0$ (initial conditions: $\theta_1 = 0.0, \theta_2 = 0.1, s_{12} = s_{21} = 0.0$); (b) $\sigma = 0.09$, $\beta_1 = \beta_2 = 0.0$, $g_{12} = g_{21} = 0.3$, $\tau_{12} = \tau 21 = 2.0, \tau_R = 0.1, \eta = 5.0$, (initial conditions: $\theta_1 = 0.0, \theta_2 = 0.01, s_{12} = 0.0, s_{21} = 0.0$) CS does not occur for this case.

of the excitatory neuron shows non-monotonic behaviour with respect to the constant input β: exhibiting very high firing frequencies at $\beta \approx 0$, then a sudden decrease at $\beta \approx 0.3$ and then a regular monotonic increase thereafter, and tending to maintain a nearly constant frequency difference with the inhibitory neuron for larger β in the deterministic system where $\sigma = 0$. The nearly constant frequency difference however is suggestive of order emerging in their phase differences with increasing β.

The plots in Figure 15 are for parameter values identical with those in Figure 6a except for the coupling which is of IE type (so that we now have now non-identical neurons): here again two different frequencies are present. In this case, for small β_i values, the large fluctuations in the frequency of the excitatory neuron (Fig. 15a) when $\sigma = 0$ arise because of the sign changes of the input $(\beta_i + \sum_{j=1}^{N} \alpha_j g_{ji} s_{ji}(\theta_j))$ since $\alpha_j = -1$; the bifurcation parameter oscillates between the stable region where $I_i < 0$ and the unstable region $I_i > 0$. Similar fluctuations are observed in the Lyapunov exponent curve also (Fig. 15b), as shown in the inset curve, and the largest exponent even becomes positive in a small window of neuronal inputs.

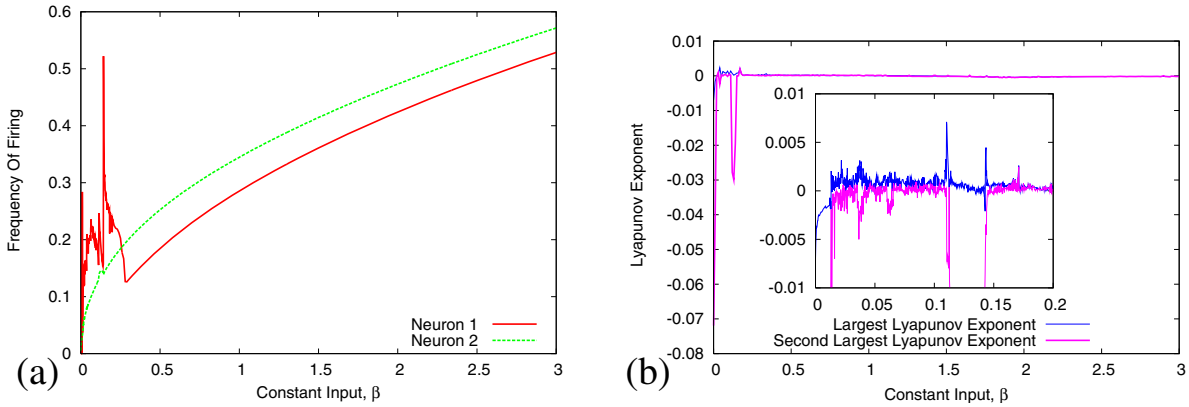

Fig. 15. (Color online) (a) Firing frequency and (b) Lyapunov exponents versus input curves for IE coupling for $\tau_{12} = \tau_{21} = 2.0, \eta = 5.0, \tau_R = 0.1$, $\sigma = 0$, $g_{12} = g_{21} = 0.3$.

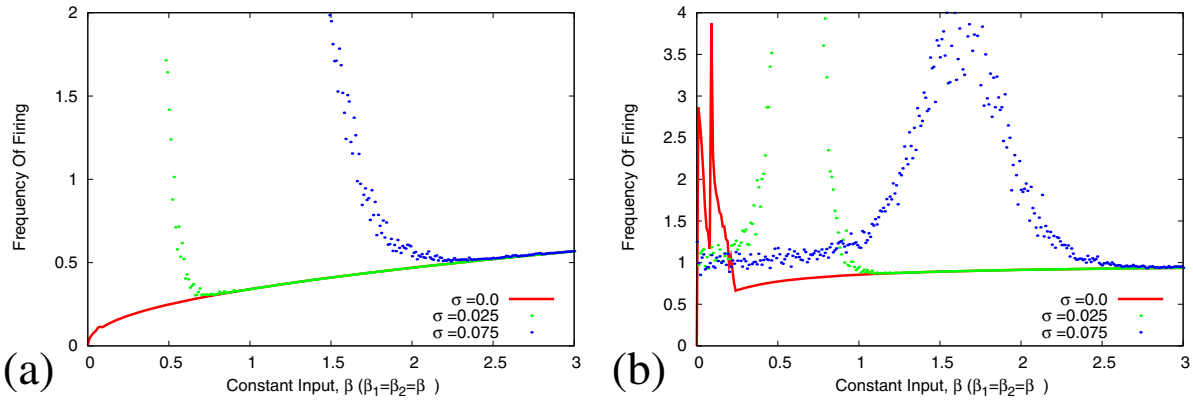

Fig. 16. (Color online) Frequency of firing as a function of constant input & effect of noise on it for IE coupling: for $\sigma = 0, \sigma = 0.025, \sigma = 0.075$. (a) Inhibitory neuron; (b) excitatory neuron.

5.4 Noise-induced variation of firing frequency and delay of bifurcation

For IE coupling, addition of noise causes the firing frequency of the inhibitory neuron to start from a high non-zero value just as in the EE case as the sign of the input term remains unchanged. However, for the excitatory neuron of Figure 15, there is a non-monotonic dependence of its firing frequency on β_i (see Figs. 15, 16b). In the absence of noise, when $\beta_i = 0$ and $\alpha_j = -1$ then $I_i < 0$ and the neuron is below the firing threshold; hence the excitatory neuron does not fire. Introduction of weak noise however injects the required energy to the neuron to overcome the threshold and fire. In Figure 16 we show that the frequency of firing in the presence of noise is higher than in the noiseless case (shown in red) but as the external input β is increased, the effect of noise on the firing frequency dies down.

We observe a very interesting phenomenon in the IE case when noise is introduced: the irregular firing of the excitatory neuron for small β_i values which was accompanied by two sharp peaks in the frequency (at the small β_i values of 0.01 and 0.1) in the absence of noise, is replaced in the presence of noise by a single broad peak at the much larger values of $\beta_i = 0.65$ for $\sigma = 0.025$, and $\beta_i = 1.6$ for $\sigma = 0.075$ (Fig. 16b). Here noise appears to *delay* the bifurcation associated with this different firing behaviour.

It is well known that the sweep of a control parameter which is slowly varying in time, causes a delay in the steady bifurcation point [23]. The effect of Gaussian white noise into such a system reduces this delay in the bifurcation point depending upon whether the noise is additive or multiplicative [24]. In equations (5) and (6) Gaussian white noise enters the system multiplicatively. The neuronal inputs especially for the IE synapse show relaxation oscillations, having slow and fast time scales. This is quite distinct from the cases studied in [24], where inputs vary very gradually and slowly with time. We note that the delay in the bifurcation associated with the change in the firing behaviour is for the *excitatory* neuron of the IE system, and not for the inhibitory neuron.

As mentioned earlier, we observe from the time series that noise causes a delay in the synaptic decay time [15]. While in the EE case this results in a change in the onset of the arrival of the maximal input values to the neurons and eventual synchronization (CS) of the neuronal outputs [15], in the IE case, because the signs of the input

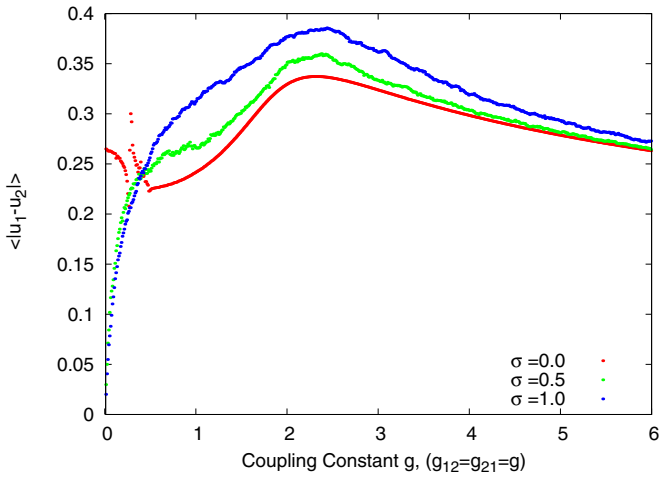

Fig. 17. (Color online) Variation of $\langle|u_1 - u_2|\rangle$ with the coupling strength $g_{12} = g_{21} = g$ for IE coupling. parameter values are: $\tau_{12} = \tau_{21} = 2.0, \beta_1 = \beta_2 = 0.1, \tau_R = 0.1$ (initial conditions: $\theta_1 = 0.0, \theta_2 = 0.01, s_{12} = 0.0, s_{21} = 0.0$).

terms of the two neurons are mutually opposite, the neurons eventually are never able to fire in-step and hence CS is almost never achieved.

Noise-induced delay of bifurcation in coupled theta neurons has been reported earlier in the literature [17], but the coupling in their case was purely of EE type.

5.5 Noise-induced synchronization and locking to partially synchronized state

For IE coupling (Fig. 17), the synchronization error $\langle|u_1 - u_2|\rangle$ has a maximum magnitude at $g_{ij} = 2.4$ approximately, for all values of noise strengths, and approaches a saturating value of 0.27 at about $g_{ij} = 6$ irrespective of the noise strength, both for $\beta_i = 0$ and for $\beta_i = 0.1$. There are three interesting things to be noted: first, values of $\langle|u_1 - u_2|\rangle$ are lower in the IE case in comparison to EE coupling, but in the IE case too there is partial synchronization for large coupling strengths. The second point is that increasing noise strength beyond a critical value $g_c = 0.4$ increases the difference between neuron outputs while below this value the difference decreases for nonzero σ, in contrast to the EE case where increasing noise strength brought down their difference. Finally, we see that for IE coupling in the noiseless situation, the variation of $\langle|u_1 - u_2|\rangle$ with g_{ij} at $\beta_i = 0.1$ is discontinuous at a small coupling strength of about $g_{ij} = 0.3$ (Fig. 17). The reason for the discontinuity is not yet clear to us.

Variation of $\langle|u_1 - u_2|\rangle$ with the input β for the IE case with $\tau_1 = \tau_2$, $\beta_1 = \beta_2 = \beta$, $g_{12} = g_{21}$ is shown in Figure 18 for different noise strengths. For the chosen values of parameters, we observe that there is a transition point at $\beta = \beta_c \approx 0.1$. For $\beta > \beta_c$, $\langle|u_1 - u_2|\rangle$ decreases with increasing σ. There is a cross-over region between $\beta = \beta_{c_l} = 0.03$ and β_c, and for $\beta < \beta_{c_l}$, $\langle|u_1 - u_2|\rangle$ increases with increasing σ. The plots show a dependence of

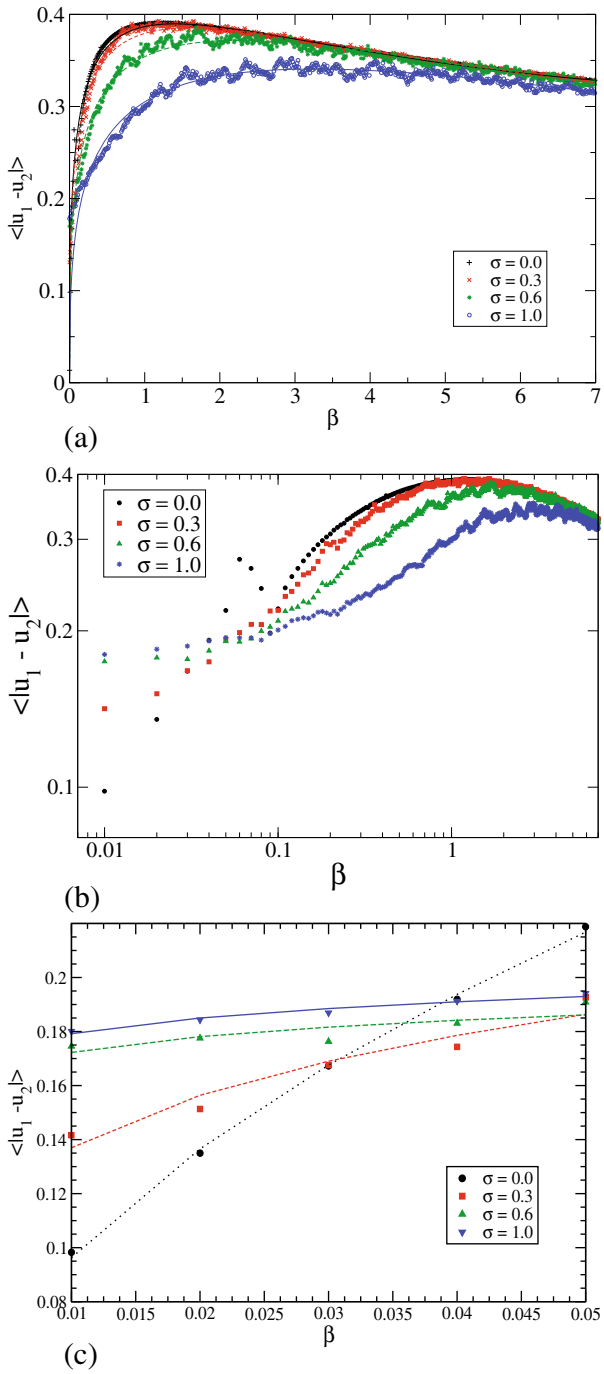

Fig. 18. (Color online) Variation of $\langle|u_1 - u_2|\rangle$ with the input $\beta_1 = \beta_2 = \beta$ for IE coupling. (a) The curves drawn on top of the data points correspond to equation (16) ($\beta > \beta_c$): k, l values associated with a given σ are: black: $\sigma = 0.0, k = 0.0564, l = -1.6731$; red: $\sigma = 0.3, k = 0.0281, l = -1.3538$; green: $\sigma = 0.6, k = 0.0092, l = -1.0569$; blue: $\sigma = 1.0, k = -0.0052, l = -0.6903$. (b) Same as (a), but on a log-log plot, clearly showing cross-over behaviour. (c) Detail of above plots in the cross-over region, curves correspond to equation (15): a, b values associated with a given σ are: black: $\sigma = 0.0, a = 0.9820, b = 0.5042$; red: $\sigma = 0.3, a = 0.3305, b = 0.1913$; green: $\sigma = 0.6, a = 0.2150, b = 0.0481$; blue: $\sigma = 1.0, a = 0.2215, b = 0.0460$. Parameter values are: $\tau_{12} = \tau_{21} = 2.0, g_{12} = g_{21} = 0.25, \tau_R = 0.1$ (initial conditions: $\theta_1 = 0.0, \theta_2 = 0.01, s_{12} = 0.0, s_{21} = 0.0$).

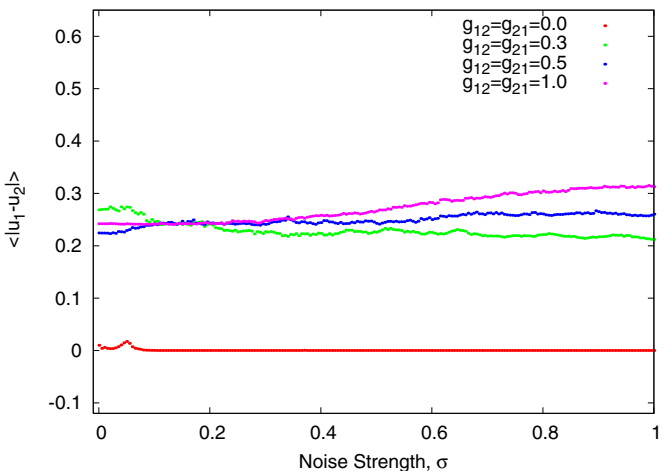

Fig. 19. (Color online) Variation of $\langle|u_1 - u_2|\rangle$ with the noise-strength σ for IE coupling. Parameter values are: $\beta_1 = \beta_2 = 0.1, \tau_{12} = \tau_{21} = 2.0, \tau_R = 0.1$ (initial conditions: $\theta_1 = 0.0, \theta_2 = 0.01, s_{12} = 0.0, s_{21} = 0.0$).

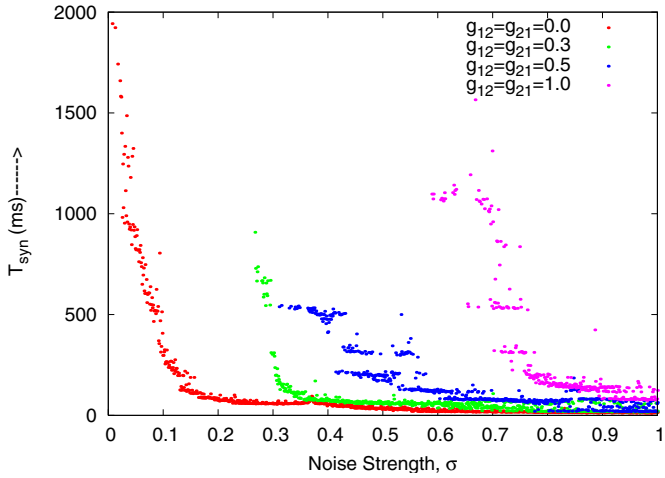

Fig. 20. (Color online) Variation of complete synchronization T_{sync} with noise strength keeping all other parameters fixed, for the EE system.

the form:

$$\langle|u_1 - u_2|\rangle \sim a\beta^b, \text{ for } \beta \leq \beta_{c_l} \quad (15)$$

where a and b vary with the noise strength σ and

$$\langle|u_1 - u_2|\rangle \sim k\beta + l\beta^{1/2} + (2-\sigma)\beta^{2/5}, \text{ for } \beta > \beta_c \quad (16)$$

where k, l vary from curve to curve and depend on the noise strength σ.

However, as mentioned earlier also, $\langle|u_1 - u_2|\rangle$ never becomes zero for IE synapses; instead, at large β_i values, the output difference saturates for all noise strengths to a limiting value of about 0.325 and the system gets locked on to this state. The discontinuity at $\beta_i = 0.1$ for the noiseless case (in red) is a reflection of very small, non-negative values of the Lyapunov exponents (Fig. 15b, inset) (discussed also in the previous section) because of the total input to the excitatory neuron oscillating between the stable regime when $I_i < 0$ and the unstable regime when $I_i > 0$, depending upon the relative strengths of β_i and $\alpha_j g_{ji} s_{ji}$, since $\alpha_j = -1$ for neuron j.

The variation of $\langle|u_1 - u_2|\rangle$ with noise strength for IE synapses at different g_{ij} values, for $\beta_i = 0.1$ is displayed Figure 19. Above a noise strength of about $\sigma = 0.15$, increasing g_{ij} increases the difference between the neuron outputs; below $\sigma = 0.15$ also the system remains far from CS, but increasing g_{ij} can bring down the difference. Comparing these IE plots with the ones in Figure 10 for EE, we see that as usual EE and IE synapses show different behaviour. The uncoupled case $g_{ij} = 0$ is shown in both plots of Figures 19, 10 for comparison.

6 Variation of synchronization time with noise strength (EE coupling)

In Figure 20 we plot the time taken by the EE system to exhibit CS as a function of the noise strength, keeping all other parameters fixed. The normal clock function available with C-programming language has been used to measure the time T_{syn} taken by the system to synchronize.

To define T_{syn}, the procedure we use is as follows. For a given value of the noise strength σ, the absolute value of the output difference $|u_1 - u_2|$ is calculated, at each instance, for a large number k of iterations ($k = 300\,000$). Once $|u_1 - u_2|$ goes to zero in, say the ith iteration, (or more accurately, when this difference can be considered to be negligible computationally – less than 10^{-6}), the system is considered to have synchronized only if for all the consecutive and remaining $(k - i)$ iterations, $|u_1 - u_2| \approx 0$ continues to hold good. When this synchronization condition is found to be satisfied, then the time (from the beginning of computation) at which $|u_1 - u_2| \approx 0$ first occurred (at the ith iteration), is considered to be the synchronization time T_{syn}.

We observe that T_{syn} is smaller for higher noise strengths. Infinitesimally small noise strengths suffice to completely synchronize two uncoupled neurons ($g_{ij} = 0$), though the time taken for this to happen may be longer. In this case, increasing noise strength causes CS to occur for very small values of T_{syn}. For increasing coupling strengths, there exist plateaus or bands of σ for which T_{syn} is the same. For stronger couplings ($g_{12} = g_{21} = 0.5$ and $g_{12} = g_{21} = 1.0$) we observe the existence of metastable states in certain regimes of noise strengths where the times taken for CS to occur can be different.

This suggests the possibility of coupled neurons utilizing the different synchronization times for encoding different features from the given inputs. Indeed, this opens up the possibility of exploiting "T_{syn} switches" in artificial neural networks for feature extraction and recognition.

7 Conclusion

We have reported in this work results of some computer studies on noise-induced complete synchronization

in systems of bidirectionally coupled type-I neurons. We have studied both EE and IE couplings. From analyses of these results, we obtain functional relations between the input strength, noise strength, coupling strengths and the distance from CS. Transitions from a completely synchronized regime to a partially synchronized state to which the system gets locked with increasing coupling strength, or with increasing input, other parameters kept constant, are observed. Similarly we observe that with increasing noise strength desynchronization yields to CS. We find that the critical noise strength where this occurs has a clear functional relationship to the coupling strength and the input. For IE coupling, we find that depending on whether the input β is less or more than a critical value β_c, the system's departure from completely synchronized to a partially synchronized state occurs very differently.

We find that Gaussian white noise can cause a delay in the bifurcation associated with the firing of the excitatory neuron when the synapse is of IE type. We suggest that relaxation dynamics of the neuronal inputs in IE systems make CS of the outputs hard to achieve even in the presence of noise. Finally, we point out the possibility of utilizing the different times for complete synchronization as switches for extracting different features in networks of neurons.

We would like to thank the anonymous referees for valuable comments and useful suggestions.

References

1. A.F. Huxley, A.L. Hodgkin, J. Physiol. (London) **117**, 500 (1952)
2. H.C. Tuckwell, *Stochastic Processes in Neurosciences* (SIAM, Philadelphia, 1989)
3. L. Morris, H. Lecar, Biophys. J. **35**, 193 (1981)
4. D. Hansel, H. Sompolinsky, Phys. Rev. Lett. **68**, 718 (1992)
5. W. Wang, G. Perez, H.A. Cerdeira, Phys. Rev. E **47**, 2893 (1993)
6. F.E.-N. Hassan, M. Paulsamy, F.F. Fernando, H.A. Cerdeira, Chaos **19**, 013103 (2009)
7. J.R. Rinzel, G.B. Ermentrout, in *Methods of Neuronal Modeling*, edited by C. Koch, I. Segev (MIT Press, Cambridge, MA, USA, 1989), pp. 135–169.
8. C.V. Vreeswijk, L. Abbott, G.B. Ermentrout, J. Comp. Neuroscience **1**, 313 (1994)
9. D. Hansel, G. Mato, C. Meunier, Neural Comput. **7**, 307 (1995)
10. B. Ermentrout, Neural Comput. **8**, 979 (1996)
11. C. Börgers, N. Kopell, Neural Comput. **15**, 509 (2003)
12. C. Börgers, N. Kopell, Neural Comput. **17**, 557 (2005)
13. E. Izhikevich, IEEE Trans. Neural Networks **10**, 499 (1999)
14. W. Lim, S.-Y. Kim, J. Korean Physical Soc. **50**, 219 (2007)
15. N. Malik, B. Ashok, J. Balakrishnan, Pramana- J. Phys. **74**, 189 (2010).
16. C. Koch, *Biophysics of Computation: Information processing in single neurons* (Oxford University Press, NY, 1999)
17. B. Gutkin, T. Hely, J. Jost, Neurocomputing **58**, 753 (2004)
18. E. Kandel, J.H. Schwartz, T.M. Jessell, *Principles of neural science* (McGraw-Hill, New York, 2000)
19. A. Pikovsky, M. Rosenblum, J. Kurths, *Synchronization: A Universal Concept in Nonlinear Sciences* (Cambridge University Press, Cambridge, 2001)
20. L.M. Pecora, T.L. Carroll, Phys. Rev. Lett. **64**, 821 (1990)
21. C. Zhou, J. Kurths, Phys. Rev. Lett. **88**, 230602 (2002)
22. V.S. Anishchenko, V.V. Astakhov, A.B. Neiman, T.E. Vadisova, L. Schimansky-Geier, *Nonlinear Dynamics of Chaotic and Stochastic Systems* (Springer-Verlag, Berlin, 2002)
23. R. Haberman, SIAM J. Appl. Math. **37**, 69 (1979)
24. C. van den Broeck, P. Mandel, Phys. Lett. A **122**, 36 (1987)